Applied Energy 321 (2022) 119357

Contents lists available at ScienceDirect

Applied Energy

journal homepage: www.elsevier.com/locate/apenergy

# Investigation of a radiative sky cooling module using phase change material as the energy storage

Soroush Kiyaee [a], Pooria Khalilmoghadam [a], Mohammad Behshad Shafii [b], Alireza Z. Moshfegh [c,d,*], Mingke Hu [e,*]

[a] Department of Energy Engineering, Sharif University of Technology, Tehran, Iran
[b] Department of Mechanical Engineering, Sharif University of Technology, Tehran, Iran
[c] Department of Physics, Sharif University of Technology, Tehran, Iran
[d] Institute for Nanoscience and Nanotechnology, Sharif University of Technology, Tehran, Iran
[e] Department of Architecture and Built Environment, University of Nottingham, University Park, Nottingham NG7 2RD, UK

## HIGHLIGHTS

- The nocturnal radiative cooling potential of a trifunctional module is introduced.
- The PCM tank keeps the temperature below the minimum 24 h ambient temperature.
- The exergy efficiency calculation of radiative sky cooling systems is proposed.
- A comparison of various PCMs is performed to find the optimal storage temperature.

## ARTICLE INFO

*Keywords:*
Radiative sky cooling
Exergy analysis
Phase change material
Passive cooling
Energy storage

## ABSTRACT

Radiative sky cooling (RSC) systems have enjoyed a privileged position in the research community due to generating cooling energy without consuming electricity using the open atmospheric window and infrared emission to the sky. However, the system's justification occurs when it reaches a temperature below the minimum 24-hour ambient temperature. This study utilizes phase change materials (PCM) as the energy storage of a hybrid daytime photovoltaic-thermal and nighttime RSC module and investigates the nocturnal cooling energy-saving potential of the system at different phase transition temperatures. After being validated by the experimental data in the literature, the simulated model was used for examining the exergy and energy efficiencies of PCMs with varying phase transition temperatures. The comparison of the exergy efficiency in the radiative sky cooling systems was performed for the first time, revealing the simultaneous effect of the temperature drop and cooling power to specify the optimal operative point of the system. Based on the climatic conditions of the simulation site, the PCM with phase transition temperatures of 18 °C revealed the peak and average exergy efficiencies of 42.8% and 33.7%, respectively. Likewise, the 23 °C PCM recorded the maximum cooling power of about 49.9 W/m$^2$, and the 15 °C PCM achieved the highest temperature drop of about 14.8 °C.

## 1. Introduction

Today, the growing global needs for energy, the disadvantages of fossil fuels, and the impacts of global warming have led to the development of renewable and low-carbon energies [1–3]. One of the major concerns associated with global warming is the rapid growth of cooling systems' energy consumption. Cooling systems consume up to 15% of the power in the world, and it is predicted that by 2050, the global energy consumption for cooling will be increased tenfold due to the increasing demands [4]. It is also expected by 2050, the greenhouse gas emitted by cooling systems will grow from 10% to 45% [5]. Therefore, it is of vital importance to reduce this energy consumption.

Radiative sky cooling (RSC) is a method that can reduce objects' temperature relative to the ambient temperature without electricity consumption. RSC modules use a passive approach to cool an object by

* Corresponding authors at: Department of Physics, Sharif University of Technology, Tehran, Iran (A.Z. Moshfegh). Department of Architecture and Built Environment, University of Nottingham, Nottingham, UK (M. Hu).
*E-mail addresses:* moshfegh@sharif.edu (A.Z. Moshfegh), mingke.hu@nottingham.ac.uk (M. Hu).

https://doi.org/10.1016/j.apenergy.2022.119357
Received 4 November 2021; Received in revised form 26 January 2022; Accepted 25 May 2022
Available online 1 June 2022

**Nomenclature**

| | |
|---|---|
| $A$ | area, $m^2$ |
| $B$ | black body spectral intensity, $W/m^2/sr$ |
| $c_p$ | specific heat capacity, J/(kg·K) |
| $\dot{E}x$ | exergy rate, J/s |
| $en$ | energy, J |
| $ex$ | exergy, J |
| $g$ | gravitational acceleration, $m/s^2$ |
| $h$ | heat transfer coefficient, $W/(m^2 \cdot K)$ |
| $k$ | thermal conductivity, W/(m·K) |
| $L$ | wall length, m |
| $\dot{m}$ | mass flow rate, kg/s |
| $P$ | power, W |
| $q$ | heat flux, $W/m^2$ |
| $\dot{Q}$ | heat transfer rate, J/s |
| $Ra$ | Rayleigh number, - |
| $T$ | temperature, °C or K |
| $u$ | fluid velocity, m/s |

*Greek letters*

| | |
|---|---|
| $\alpha_p$ | thermal expansion coefficient, 1/K |
| $\varepsilon$ | emissivity, - |
| $\eta$ | efficiency, % |
| $\mu$ | dynamic viscosity, Pa·s |
| $\rho$ | density, $kg/m^3$ |
| σ | Stefan-Boltzmann constant, $W/(m^2 \cdot K^4)$ |

*Abbreviation and subscripts*

| | |
|---|---|
| a | ambient air |
| atm | atmosphere |
| bb | black body |
| con | convective |
| e | emitter |
| i | mesh number |
| ie | ideal emitter |
| in | inlet |
| ins | insulator |
| j | spectral range number |
| m | total number of spectral ranges |
| MCP | maximum cooling power |
| n | total number of meshes |
| out | outlet |
| PCM | phase change material |
| PVT | photovoltaic-thermal |
| RC | radiative cooling |
| RSC | radiative sky cooling |
| r | radiative |
| TPT | Tedlar-Polyester-Tedlar |
| w | water |

transferring a portion of the thermal radiation to outer space whose temperature is about 3 K [6,7]. This process uses the open atmospheric window in the infrared band ranging between 8 and 13 μm [8]. A thorough review of RSC technologies has been presented by Liu et al. [9]. Generally, RSC can provide an average of 40–80 $W/m^2$ net cooling power in a clear night sky [10].

RSC has long been limited to nighttime operation, aiming at reaching a temperature lower than the ambient temperature [11–14]. Daytime RSC had been left as a big challenge for decades due to the unavailability of materials with extremely low absorption in the solar radiation spectrum (0.3–2.5 μm) and high emissivity in other wavelengths, especially in the range of atmospheric window. Numerous studies have been conducted concerning the materials and structures appropriate for the radiative cooling surface, focusing on RSC during the daytime [4,15]. Chen et al. reported a temperature drop of 42 °C at noon [16], utilizing a vacuum chamber without liquid cooling. However, even an excellent emitter with ultra-low solar absorption at a favorable location may not constantly produce cooling power during the daytime. Zhao et al. [17] used a radiative cooling module to reduce the water temperature under the stationary condition, while the water temperature under the panel was the same at 4:00 PM as it was at 11:30 AM. Therefore, from the point of view of energy efficiency, it is better to produce heat in the daytime and cooling in the nighttime. A photovoltaic-thermal RSC (PVT-RSC) module can generate electricity and thermal power during the day and cooling power at night. Since photovoltaic solar cells generally have a high emissivity in the infrared range, the generation of heat and electricity during the day and cooling at night can be performed.

Vall et al. [18] experimentally tested the combination of solar thermal collector and radiative cooler with the idea of an adaptive coating, which provides high spectral transmittance in the solar radiation band and high spectral emissivity in the atmospheric window range. During the night, the system achieved a maximum cooling power of 33 $W/m^2$, with an average cooling efficiency of 32%. A mathematical model was developed by Hu et al. [19] to evaluate the nocturnal performance of a PV/T module and determine its overnight cooling capacity. Under optimal conditions, the absorber plate could reach a temperature of approximately 11 °C below ambient temperature and exceed a maximum cooling power of 50 $W/m^2$. Bokor et al. [20] utilized a transpired solar collector for nocturnal radiative sky cooling. The collector plate could cool down the ambient air up to 4.0 °C. The system's peak and average cooling performance were reported to be 66.5 $W/m^2$ and 34.6 $W/m^2$, respectively.

The main problem of the studies on RSC is the lack of attention to the minimum ambient temperature of day and night. Only the ability to reduce the water temperature passing through the module has been addressed, while the temperature of the water outlet from the module at most hours of day and night is higher than the minimum 24-hour ambient temperature. Indeed, the system in these hours constitutes no achievement because the temperature of an outdoor open and non-thermal insulated water tank could be minimized at midnight without using an RSC panel and by merely natural cooling. Therefore, the system potential must be focused on reducing the storage temperature to lower than the minimum ambient temperature or tap water temperature throughout the day.

In this study, we used phase change materials (PCM) with phase transition temperatures less than the minimum ambient temperature that helps to store the cooling energy at a specific temperature. Several studies have been conducted on PCM utilization to store solar thermal energy [21–23] or remove room sensible heat [24–26], but their application in RSC systems to achieve a temperature lower than ambient has not been researched. Since PCM can keep lots of energy at the phase transition temperature, a low mass of the storage tank will be sufficient. As a result, the tank's temperature will decrease quickly to the phase transition temperature. This helps the storage tank reach the optimal temperature even on cloudy nights in which the cooling power is low. Therefore, a PCM tank is always available with the desired temperature.

In the papers published so far, the cooling power, energy efficiency, and maximum temperature drop have been reported [27–29]. However, these criteria alone are not sufficient for the comparison because the cooling energy quality (the temperature drop along with the cooling power) is not considered. Cooling power is directly proportional to energy efficiency and inversely proportional to the maximum temperature drop. Consequently, the peak radiative cooling power is generated when there is no temperature reduction, and by an intense temperature drop,

the cooling power will be reduced considerably. Thus, we calculated the exergy efficiency, including the effects of temperature drop and cooling power simultaneously. It is a more appropriate criterion to compare the results of different RSC systems.

In the present study, four PCMs are used to compare storing cooling energy in the nighttime. Even though the system can generate electricity and thermal energy during the day, we focus on producing cooling power at night. The simulation is conducted by Comsol Multiphysics software after model validation using two experimental papers [30,31].

## 2. System design and input parameters

### 2.1. Model description and assumptions

The outline of the PVT-RSC module and the PCM storage tank is shown in Fig. 1. The water passing through the panel during the night is cooled by radiative cooling, and then it is directed to the PCM storage tank. The storage walls and the back of the panel are covered with a 5 cm polyurethane foam insulation, and its thickness at the bottom and top of the panel is 3 cm. The PCM tank consists of 8 slabs with a total mass of 10 kg. The thermodynamic properties of PCMs will be described in Section 2.2. The water flow in the system is maintained as long as the water temperature is less than the average PCM temperature. Thus, the PCM temperature will decrease, and after reaching the phase transition temperature, it will enter the solid phase and freeze. This study aims to compare PCMs with different phase transition temperatures for the storage tank. The following assumptions are considered in the simulation model:

The PCM storage tank and PVT-RSC module are simulated in two dimensions, and due to symmetry, the heat transfer along the Z-axis is ignored.
In the experimental conditions, the water flow below the module is cooled by copper pipes. However, since the simulation has two dimensions, the flowing water is considered planar under the aluminum plate.
The inlet water temperature of the PCM storage tank is considered equal to the outlet water of the module.
The water flowing through the module and storage is considered laminar and fully developed.
The depth of the module along the Z-axis is 1 m, and its length is also 1 m. Therefore, the results are reported for an area of 1 $m^2$.
The external surfaces of the module and storage insulations are covered by a layer like aluminum foil whose emissivity is less than 0.05 to reduce the wasted energy. Therefore, the transfer of radiative heat by these surfaces to the environment is ignored.
The initial temperature of the module equals the ambient temperature, and the initial temperature of PCM storage tanks equals tap water temperature, which is almost constant during the simulation period. It varies between 30 °C and 30.2 °C. Since this study's purpose is to cool the storage tank, choosing the tap water temperature as a free temperature source with a lower temperature than ambient is preferable.

To ensure the assumed simplifications, the validation of the model in Section 4 is done under the conditions mentioned above. The rest of the assumptions are discussed in the following.

### 2.2. PCMs thermodynamic properties

The inner part of the storage tank consists of six PCM slabs that aim to store cooling energy at the phase transition temperature. Since the higher the specific latent heat (assuming the mass and specific heat capacity are constant), the more energy is stored in the storage tank, we used PureTemp bio-based PCMs [32] with a latent heat of 187 kJ/kg in the temperature range of 15 °C to 23 °C. Although there is a slight

**Table 1**
Physical properties of PCMs [32].

| Phase transition temperatures (°C) | Density ($kg/m^3$) | Specific latent heat capacity (kJ/kg) | Specific heat capacity (J/kg.K) | Thermal conductivity (W/m.K) |
|---|---|---|---|---|
| 15-18-20-23 | 860 | 187 | Liquid: 2146<br>Solid: 1924 | Liquid: 0.15<br>Solid: 0.25 |

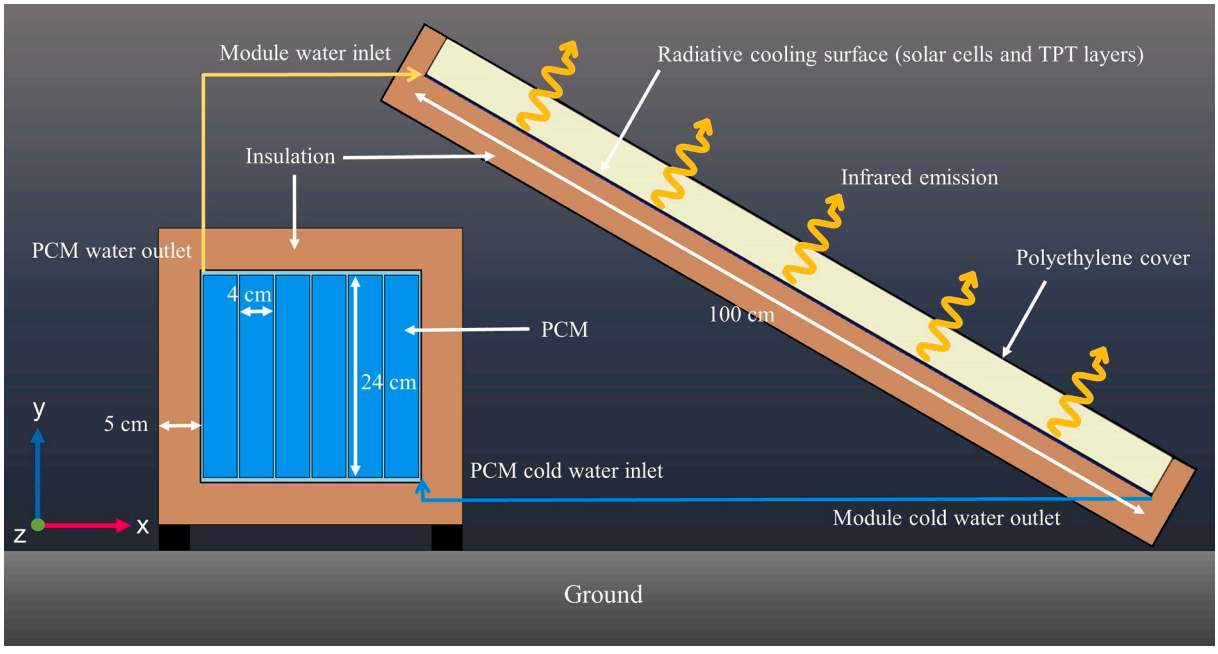


**Fig. 1.** The cooling process of the PVT-RSC module at night. The cold water leaving the module is directed to the PCM storage tank, and after transferring the cooling energy, it is directed to the module again to form a closed cycle. Solar cells and Tedlar-Polyester-Tedlar (TPT) layers act as the radiative cooling surface.

difference in PCMs' thermodynamic properties, for better comparison, they are considered similar except for the phase transition temperature (Table 1). It is important to note that the PCM phase transition does not occur suddenly at the phase transition temperature. This happens in a temperature range of about 4°. For instance, 18 °C PCM is frozen in the temperature range of 16 °C to 20 °C.

### 2.3. Ambient properties

Hundreds of years ago, mud-brick Yakhchals (ice houses) were used in hot and dry areas of central Iran, such as the city of Yazd [33]. This city is selected for simulation since it has low relative humidity and open atmospheric window at night. This study considers the ambient parameters, including temperature, relative humidity, and atmospheric emissivity.

Fig. 2 shows the temperature and relative humidity in one clear summer night [34] (July 24 and 25, 2021). We used MODTRAN mid-latitude summer model [35] to estimate the atmospheric emissivity in the infrared range. Fig. 3 shows the emissivity diagram in the wavelength range of 2–20 μm with a step size of 1 μm at different test hours during the night. In the other bands, the atmospheric emissivity is considered equal to one.

### 2.4. Radiative surface emissivity

To investigate the emissivity of the PVT-RSC module surface, two ideal emitters shown in Fig. 4 are compared. Until a specific temperature of the emitter, emitter 2 has a greater cooling power than emitter 1. In the study conducted by Huang et al. [36], this temperature is 20 °C lower than the ambient temperature. The temperature drop of more than 20 °C will result in the superiority of the emitter 1 over the other one. But it is essential to note that the lower the emitter temperature than the ambient temperature, the more the wasted energy, and the lower the system energy efficiency. In the present study, energy and exergy efficiencies are crucial; therefore, a high-temperature reduction close to the stagnation state is not desired. The stagnation state is reached when the system experiences the greatest temperature drop and the net cooling power reaches zero. In this condition, the ideal emitter 2 is a preferable option. In addition, since RSC is only performed at night in this study, high spectral emissivity (absorptivity) in the solar spectrum is not an obstacle but improves electrical and thermal efficiencies during the daytime. Therefore, the best emitter is the one with maximum emissivity all over the ultraviolet, visible, and infrared spectra. We used the surface

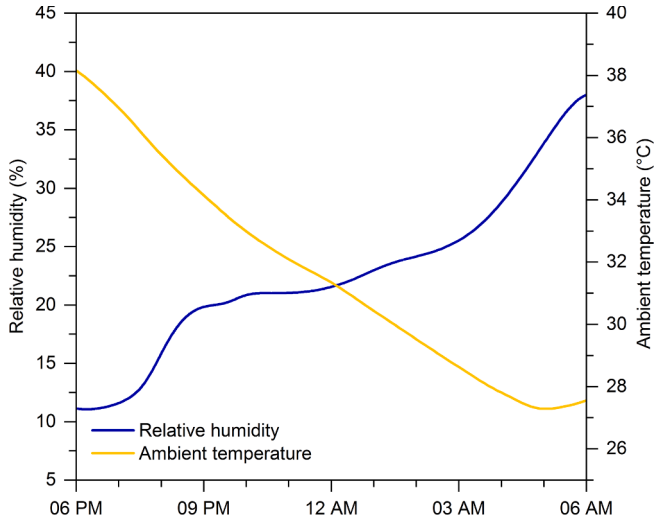


**Fig. 2.** Temperature and relative humidity on July 24 and 25, 2021, Yazd, Iran [34].

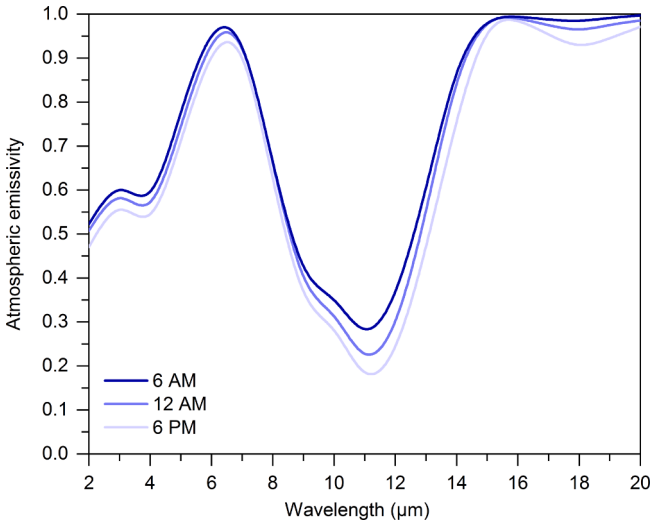


**Fig. 3.** Calculated atmospheric emissivity at night in three different hours on July 24 and 25, 2021, Yazd, Iran.

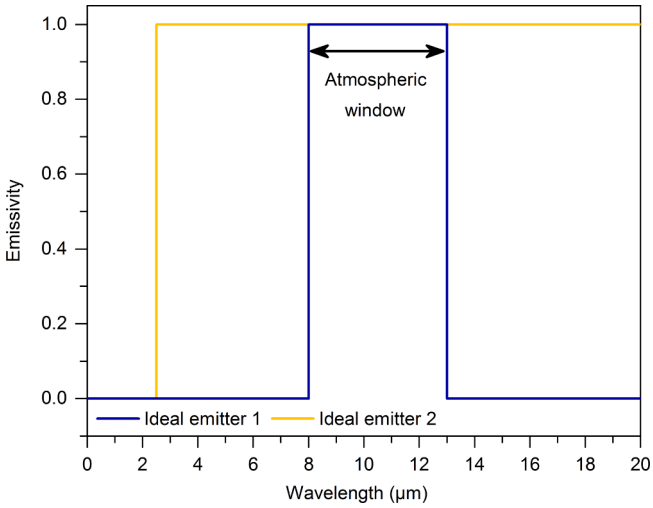


**Fig. 4.** Surface emissivity of two different ideal emitters.

properties studied by Zhao et al. [37] in the PVT-RSC module. Its average emissivity is considered to be 0.95 in the range of 3–20 μm and assumed to be 0.9 in the range of 0.3–3 μm.

### 2.5. Cover transmissivity

One of the most critical factors that have affected the applicability of RSC systems is the lack of a rigid and robust cover with high transmission in the mid-infrared and visible spectrum [9]. Despite low strength, ultra-thin polyethylene is still the best choice among the available materials because its transmission is high in both infrared and visible spectrums. Hu et al. [38] reported the spectral transmittance of a low-density polyethylene film with a thickness of 20 μm, which transmits about 90% of the radiation spectrum in the range of atmospheric window.

## 3. Simulation model

### 3.1. Thermal energy model

The PVT-RSC module is cooled by radiation towards the sky during the night, and its cooling power is transferred to the PCM storage tank.

The model simulation is carried out in Comsol Multiphysics software with a time-dependent study. The software uses a partial differential equation to calculate the panel and storage tank temperature, as follows [39]:

$$\rho C_p \frac{\partial T}{\partial t} + \rho C_p u.\nabla T + \nabla.\boldsymbol{q} = Q \tag{1}$$

where ρ denotes the material density, $T$ is the temperature, $C_p$ is the specific heat capacity at constant pressure, $u$ is the fluid velocity vector,$Q$ is the heat source, and $\boldsymbol{q}$ is the heat flux, which is calculated by Eq. (2).

$$\boldsymbol{q} = -k\nabla T \tag{2}$$

where $k$ is the material thermal conductivity. The convective heat flux is computed using the following equations:

$$-n.\boldsymbol{q} = q_{con} \tag{3}$$

$$q_{con} = h(T_a - T) \tag{4}$$

$q_{con}$ is the convective heat flux, n is the normal vector toward the exterior surface, $h$ is the convective heat transfer coefficient, and $T_a$ is the ambient temperature. Eqs. (5)-(8) calculate the convective heat transfer coefficients of horizontal, vertical, and inclined walls for the module and storage tank based on the equations proposed by Incropera et al. [39,40]:

$$h_{horizontal,upside} = \frac{k_a}{L} 0.27 Ra^{\frac{1}{4}} \tag{5}$$

$$h_{horizontal,downside} = \begin{cases} \frac{k_a}{L} 0.27 Ra^{\frac{1}{4}}, Ra \le 10^9 \\ \frac{k_a}{L} 0.27 Ra^{\frac{1}{4}}, Ra > 10^9 \end{cases} \tag{6}$$

$$h_{vertical} = \begin{cases} \frac{k_a}{L}\left(0.68 + \frac{0.67(Ra)^{\frac{1}{4}}}{\left(1+\left(\frac{0.492k_a}{\mu C_p}\right)^{\frac{9}{16}}\right)^{\frac{4}{9}}}\right), Ra \le 10^9 \\ \frac{k_a}{L}\left(0.825 + \frac{0.387(Ra)^{\frac{1}{6}}}{\left(1+\left(\frac{0.492k_a}{\mu C_p}\right)^{\frac{9}{16}}\right)^{\frac{8}{27}}}\right)^2, Ra > 10^9 \end{cases} \tag{7}$$

$$h_{inclined} = \begin{cases} \frac{k_a}{L}\left(0.68 + \frac{0.67(\cos\varphi Ra)^{\frac{1}{4}}}{\left(1+\left(\frac{0.492k_a}{\mu C_p}\right)^{\frac{9}{16}}\right)^{\frac{4}{9}}}\right), Ra \le 10^9 \\ \frac{k_a}{L}\left(0.825 + \frac{0.387(\cos\varphi Ra)^{\frac{1}{6}}}{\left(1+\left(\frac{0.492k_a}{\mu C_p}\right)^{\frac{9}{16}}\right)^{\frac{8}{27}}}\right)^2, Ra > 10^9 \end{cases} \tag{8}$$

where $L$ is the wall length, $\varphi$ is the angle between wall and vertical direction), $C_p$ is the specific heat capacity of air at constant pressure,$\mu$ is the air dynamic viscosity, and $k_a$ is the thermal conductivity of air. Eq. (10) determines the Rayleigh number, $Ra$ [39].

$$Ra = \frac{g\alpha_p \rho^2 C_p \left|T_{i,ins} - T_a\right| L^3}{k_a \mu} \tag{9}$$

$\rho$ is the air density, $g$ is the gravitational acceleration, and $\alpha_p$ is the coefficient of thermal expansion, which is calculated as follows [39]:

$$\alpha_p = -\frac{1}{\rho}\left(\frac{\partial \rho}{\partial \overline{T}}\right)_p \tag{10}$$

$$\overline{T} = \frac{T_{i,ins} + T_a}{2} \tag{11}$$

The radiative heat flux is calculated using Eqs. (12) and (13).

$$-n.\boldsymbol{q} = q_r \tag{12}$$

$$q_r = A_e \varepsilon_e \pi \sum_{j=1}^{m} \varepsilon(atm,j) B(T_a,j) - A_e \varepsilon_e \sigma T_e^{\,4} \tag{13}$$

where $q_r$ is the radiative heat flux, $A_e$ is the area of the radiative cooling module surface,$\varepsilon_e$ is the emitter surface emissivity, $\varepsilon(atm,j)$ is the atmospheric emissivity in the spectral range of the number $j$,$B$ is the black body spectral intensity, σ is the Stefan-Boltzmann constant, $T_e$ is the emitter temperature, and $m$ is the number of the spectral range considered for the atmosphere.

### 3.2. Energy efficiency

In energy systems, the energy efficiency is calculated by dividing the useful energy by the total input energy. As a result, in an RSC system, it can be defined by the ratio of the absorbed cooling power to the maximum cooling power the system can achieve. The cooling power absorbed by PCM is determined by Eqs. (14) and (15).

$$P_{PCM} = P_{module} - P_{loss} \tag{14}$$

$$P_{module,c} = \dot{m} c_{p,w} (T_{in,w} - T_{out,w}) \tag{15}$$

where $P_{module}$ is the water cooling power of the module, $P_{loss}$ is the wasted power by PCM storage insulated walls, $\dot{m}$ is the water mass flow rate through the module, $c_{p,w}$ is the specific heat capacity of water, $T_{out,w}$ is the module outlet water temperature, and $T_{in,w}$ is the module inlet water temperature. Since the external surfaces of the storage are divided into n elements by meshing, the wasted power can be computed by Eq. (16).

$$P_{loss} = \sum_{i=1}^{n} A_i h_{i,ins} (T_a - T_{i,ins}) \tag{16}$$

$A_i$, $T_{i,ins}$ and $h_{i,ins}$ are the area, temperature, and convective heat transfer coefficient of the i$^{th}$ mesh, respectively. The system cooling energy efficiency could be calculated by the following equation:

$$\eta_{en} = \frac{P_{PCM}}{P_{bb,T_e}} \times 100 \tag{17}$$

where $P_{bb,T_p}$ is the cooling power of a black body with an area and instantaneous temperature equivalent to the emitter surface used in the module. This is the maximum cooling power of a material at the emitter surface temperature.

### 3.3. Exergy efficiency

Eq. (18) shows the exergy rate balance of the PCM storage tank.

$$\dot{E}x_{in} - \dot{E}x_{out} - \dot{E}x_{loss} - \dot{E}x_{PCM} = 0 \tag{18}$$

$\dot{E}x_{in}$ is the exergy rate of the storage inlet water, $\dot{E}x_{out}$ is the exergy rate of the storage outlet water, $\dot{E}x_{loss}$ is the exergy loss rate from storage walls, and $\dot{E}x_{PCM}$ is the rate of the cooling exergy stored in PCM. The exergy loss rate from storage boundaries can be expressed according to:

$$\dot{E}x_{loss} = \int_{storageboundaries} \left(\frac{T_a}{T_{ins}} - 1\right) d\dot{Q} \tag{19}$$

$T_{ins}$ is the insulator outer surface temperature, and $\dot{Q}$ is the heat

transfer rate from insulator to the ambient. Eq. (19) is inspired by the exergy rate due to heat transfer based on the Carnot factor [41].

The system exergy efficiency and the storage inlet and outlet exergies are calculated as follows [9]:

$$\eta_{ex} = \frac{\dot{E}x_{PCM}}{\dot{E}x_{atm}} \times 100 = \frac{\dot{E}x_{in} - \dot{E}x_{out} - \dot{E}x_{loss}}{\dot{E}x_{atm}} \times 100 \tag{20}$$

$$\dot{E}x_{in} = \dot{m}c_{p,w}[T_a + T_a \ln\left(\frac{T_{in}}{T_a}\right) - T_{in}] \tag{21}$$

$$\dot{E}x_{out} = \dot{m}c_{p,w}[T_a + T_a \ln\left(\frac{T_{out}}{T_a}\right) - T_{out}] \tag{22}$$

where $\dot{E}x_{atm}$ is the maximum rate of the exergy entering the system from the atmosphere, calculated by Eq. (23).

$$\dot{E}x_{atm} = MCP(\frac{T_a}{T_{sky}} - 1) \tag{23}$$

$T_{sky}$ is the sky temperature, and MCP is the maximum cooling power of the ideal emitter, calculating as below:

$$MCP = P_{ie}(T_e) - P_{atm}(T_a) = A_e\varepsilon(bb)\sigma {T_e}^4 - A_e\varepsilon(bb)\pi \sum_{j=1}^{m} \varepsilon(atm,j)B(T_a,j) \tag{24}$$

$P_{ie}(T_e)$ is the ideal emitter radiation power at the average temperature of the emitter surface, $P_{atm}(T_a)$ is the atmospheric radiation power on the emitter surface at the ambient temperature, and $\varepsilon(bb)$ is the black body emissivity which is equal to 1.

Eq. (23) is inspired by the exergy equation of the Sun in calculating the thermal exergy efficiency of solar collectors [42]. In calculating the Sun exergy rate, its temperature is used as the hot energy source, which is the hot source temperature in a Carnot heat engine. In contrast, sky temperature is used in Eq. (23) as the cold place temperature in heat pumps and refrigeration systems [43]. Different models are proposed to calculate the sky temperature, but since in this study we have computed atmospheric emissivity in various spectral ranges, the sky temperature could be calculated by Eq. (25).

$$\pi \sum_{j=1}^{m} \varepsilon(atm,j)B(T_a,j) = \sigma {T_{sky}}^4 \tag{25}$$

The sky temperature is the minimum surface temperature that the ideal emitter 2 –that was mentioned in section 2.4– can reach. If the selected emitter is the ideal emitter 1, this minimum temperature will decrease, and it must be evaluated using other equations.

## 4. Model validation

### 4.1. RSC module

The RSC simulation model is validated by the experimental results presented by Hu et al. [30] to ensure the simulation steps. A module with an area of 2 $m^2$ was used in their study to produce coldness, heat, and power. Silicon solar cells covered by TPT layers cool the water in the nighttime due to high emissivity in the infrared range. A 2D geometry with all the assumptions presented in Section 2.1 is utilized to simulate the RSC plate. However, the 120-litre water tank used in the experimental system is considered cylindrical in a 3D geometry. The water flow rate of 0.038 kg/s was maintained during the test period. Fig. 5 compares the temperature of the water tank, panel inlet and outlet water measured by Hu et al. with the present simulation. To evaluate the simulation quality, the root mean square error (RMSE) is employed, which is calculated using the following equation [44]:

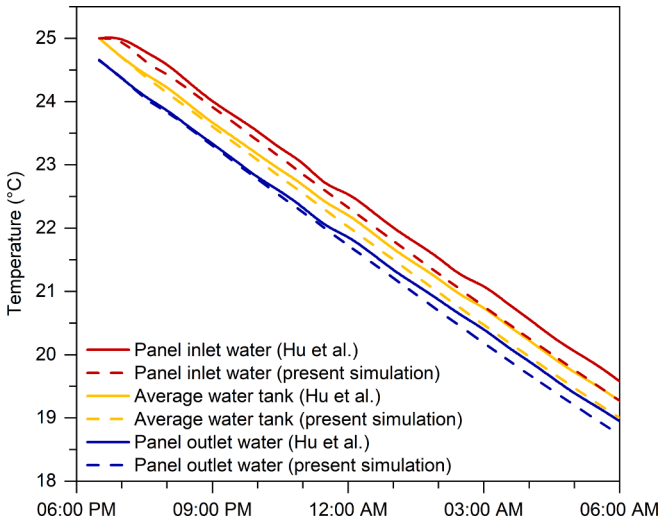


**Fig. 5.** Comparison between the experimental results of Hu et al. [30] and present simulation.

$$RMSE = \sqrt{\left[\frac{1}{N}\sum_{i=1}^{N}(T_e - T_s)^2\right]} \tag{26}$$

where $T_e$ is the experimental water tank temperature, $T_s$ is the water tank temperature in the present simulation model, $i$ is the time step, and $N$ is the evaluated time steps. The maximum RMSE of 1.5 °C for the operating temperature is specified in the German standard VDI 6020 [31]. Thus, if the RMSE value is calculated to be less than 1.5 °C, a reasonable match between the simulation and experimental results is achieved. The RMSE for inlet, outlet, and average water tank temperature is calculated as 0.22 °C, 0.14 °C, and 0.18 °C, respectively. It should be noted that the assumptions for validation are the same as those mentioned in Section 2.1.

### 4.2. PCM tank

The experimental result reported by Gallardo and Berardi [31] is used to validate the PCM phase transition simulation. In their study, a radiant ceiling panel was developed using PCM for cooling applications. PCM can be frozen passively or by energy consumption during non-peak hours, and this stored cooling energy can be used to lower the room temperature during other hours.

To ensure the validity of the simulation results, a small test chamber was used to mimic an actual test room. The insulated chamber with Rockwool is shown schematically in Fig. 6a. At the bottom is a metal plate with a constant temperature of 26 °C, representing the room temperature. An 8 mm thick layer of cellular rubber is placed on the metal plate to establish a heat transfer coefficient of 10 W/$m^2$.K between the heat source and PCM. The CrodaTherm21 PCM with a mass of 2 kg, a phase transition temperature of 21 °C, and latent heat of 190 kJ/kg is placed in the chamber's center [45]. The initial temperature of the system is set at 15 °C, and PCM is completely frozen. For 13 h, heat is transferred to the system via the metal plate to measure the PCM temperature over time. During this time, no water flow is established in the system. Although only the melting curve of PCM is reported in their study, it can still validate the phase transition process. Fig. 6b shows the temperature diagram at the bottom of PCM in the experimental test of Gallardo and Berardi and the simulation result in this study. The RMSE value is calculated as 0.35 °C, indicating an acceptable agreement between the two data.

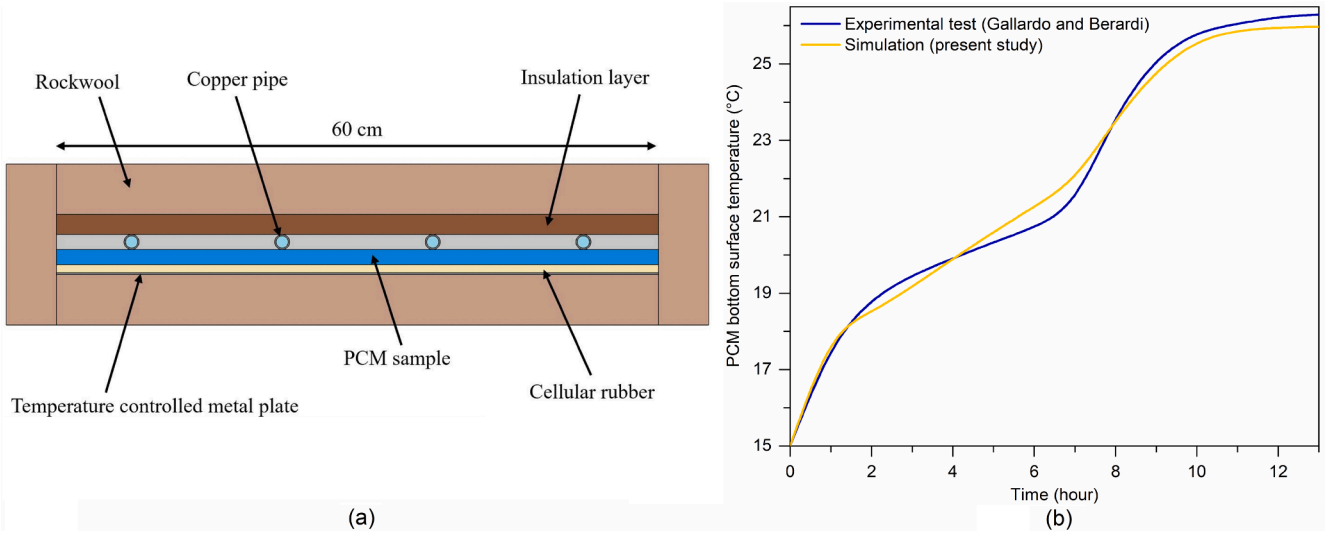


**Fig. 6.** (a) The test chamber utilized by Gallardo and Berardi [31] (b) PCM temperature measured in the experimental test and present study simulation.

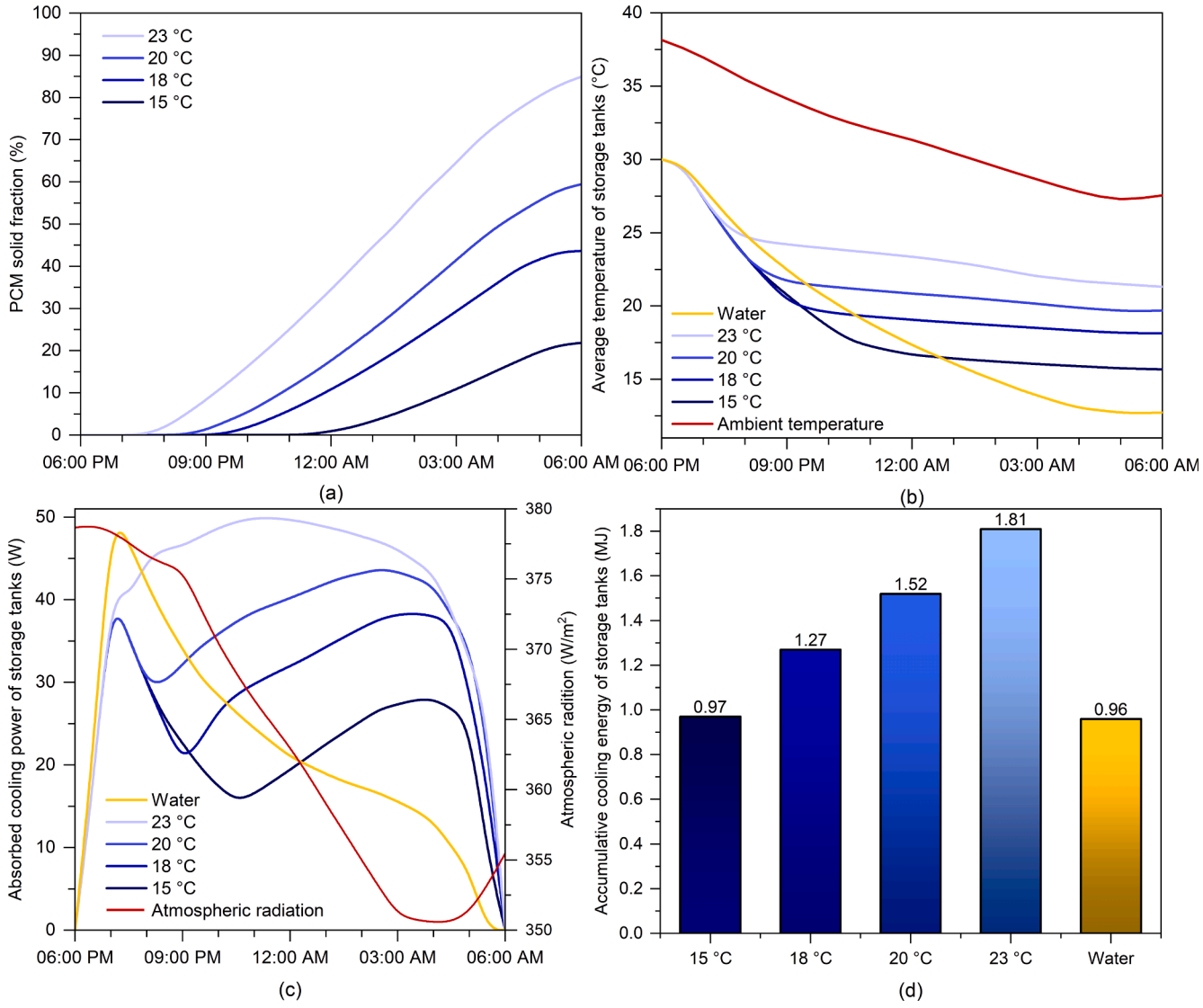


**Fig. 7.** (a) The solid fraction, (b) absorbed cooling power, (c) average temperature, and (d) accumulative cooling energy of different PCMs.

## 5. Results and discussions

The system simulation is performed from 6 PM on July 24 to 6 AM on July 25 to generate cooling power. Water and four PCMs are used in a storage tank for comparison study. The mass value of 10 kg for the storage tank is chosen because more than 80% of the 23 °C PCM (i.e., the PCM with the phase transition temperature of 23 °C) freezes with this mass. The optimal value of the water flow rate through the PVT-RSC module and storage tank is assumed to be 10 $cm^3/s$, which is determined by trial and error to maximize PCMs' solid fraction. Fig. 7a shows the solid fraction of each storage tank. Since the 23 °C PCM maintains the system's average temperature closer to ambient temperature, it has less wasted energy than other PCMs. It receives more cooling power from the panel, and a more significant portion of PCM turns into the solid phase.

Fig. 7b demonstrates the average temperature of each storage tank. Since the water tank has a higher specific heat capacity than PCMs, it has a lower temperature drop in the early two hours. While after that, PCM tanks remain at around their phase transition temperature, and the water tank continues its temperature drop.

Fig. 7c shows an increasing trend in the absorbed cooling power of the storage tanks during the first hour. When nighttime cooling begins, a significant portion of the cooling power is spent to lower the panel temperature, 38 °C. In comparison, the initial temperature of the storage tank is assumed to be 30 °C, which is the temperature of the tap water. Therefore, in the initial phase, most of the cooling power is absorbed by the panel, and the cooling power absorbed by the tank is small. A decreasing trend is observed after 7 AM in all tanks except 23 °C PCM due to their temperature reduction—the lower the system temperature, the lower the cooling power. As 23 °C PCM approaches its phase transition temperature and its temperature does not drop considerably, this decrease in absorbed cooling power is not observed. This declining trend continues until the phase transition temperature of the PCM tanks is reached. Since the water tank does not freeze, this decrease continues until the end of the simulation period. After reaching the phase transition temperature range, the tank temperature changes with a lower slope. As the ambient temperature shows a decreasing trend at this moment (Fig. 2), the absorbed cooling power of the PCM tanks takes an upward trend. If all system parameters in an RSC system remain constant, the cooling power will increase as the ambient temperature decreases.

Another variable that affects cooling performance is incoming atmospheric radiation. It has a descending tendency until 4 AM, and a peck in cooling power is observed in 15 °C, 18 °C, and 20 °C PCM tanks.

Fig. 7d illustrates the accumulative cooling energy of various tanks. Since the 23 °C PCM absorbs the highest cooling power during the day, it

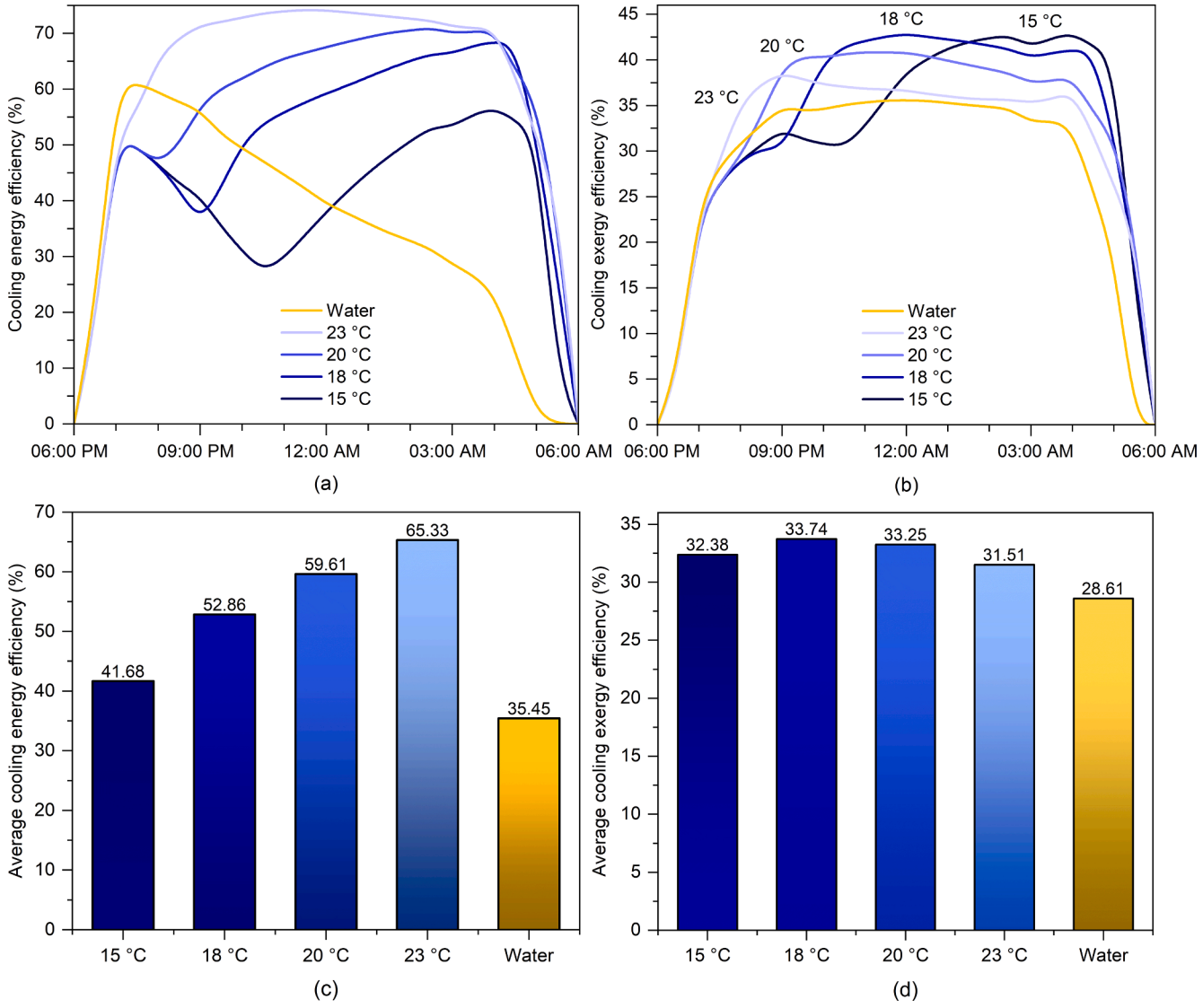


**Fig. 8.** (a) Cooling energy, (b) cooling exergy, (c) average cooling energy, and (d) average cooling exergy efficiencies of water and PCM storage tanks.

has the maximum value of accumulative cooling energy equal to 1.81 MJ. The water tank recorded the lowest value of 0.96 MJ, close to 15 °C PCM tank.

Choosing a PCM with a lower phase transition temperature decreases the absorbed cooling power but increases the temperature drop, providing the consumer with a colder storage temperature. Naturally, the cooling energy efficiency will be reduced by the decrement of the absorbed cooling power. A PCM with a lower phase transition temperature has the advantage of colder water, but on the other hand, it has a lower energy efficiency (Fig. 8a). In this condition, to choose the optimal temperature, it is required to compare the exergy efficiency shown in Fig. 8b. Although the 23 °C PCM has the highest average cooling energy efficiency (Fig. 8c), it has the lowest average exergy efficiency among other PCMs (Fig. 8d). On average, 18 °C PCM has a higher exergy efficiency than other cases, and it is the optimal point for selecting the phase transition temperature. In the case of this PCM, the maximum temperature drop relative to the ambient is 13.8 °C around 9 PM, and the maximum absorbed cooling power is 38.3 W/m$^2$ at 3:30 AM. In contrast, the 23 °C PCM has the greatest cooling power (49.9 W/m$^2$), and the 15 °C PCM has the most significant temperature drop (14.8 °C). Even though the water tank has the lowest final temperature, its average energy and exergy efficiencies are lower than all PCMs tanks.

Since the 18 °C PCM has the highest exergy efficiency, we compared its discharge during the day with that of the water tank. As shown in Fig. 7b, the water tank temperature is about 5 °C cooler at the end of the simulation, making the water tank appears a better choice over PCM. The difference, however, becomes apparent when the cooling energy of both tanks is discharged. To discharge the tanks, 30 °C tap water flows at 10:24 AM, when the ambient temperature is 35 °C. The water flow rate is 10 cm$^3$/s, the same as the flow rate during the charging process. Fig. 9 shows the temperature diagram of the outlet water of the PCM and the water tank. Except for the first half-hour, the outlet temperature of the PCM tank is lower than that of the water tank. The water tank loses its low temperature quickly, but it happens more slowly in the PCM tank because it has a higher quality of cooling energy stored in it. In other words, it has a higher exergy efficiency. To achieve a lower water outlet temperature, the total area of the module, the flow rate, or the tank volume can be changed.

According to the stated results, it would be challenging to choose the optimal storage tank without using the concept of exergy efficiency. The investigation of exergy efficiency in RSC systems could be a better comparison that examines the amounts of cooling power and temperature drop simultaneously.

## 6. Conclusions

This study aimed to investigate the application of a PCM storage tank for cooling purposes based on radiative sky cooling at night. The simulation was done on a summer night by using the meteorological information of Yazd, Iran.

By using a PCM, the cooling energy is stored at a specific temperature equivalent to the phase transition temperature. In the studies concerning RSC, the values of cooling power and maximum temperature drop are regularly recorded. However, they have limitations when assessing the cooling performance of a RSC system because the maximum cooling power is achieved when there is no temperature drop (no cooling effect) and vice versa. Therefore, we presented the calculation method of exergy efficiency in the RSC system to determine the optimum PCM phase transition temperature by a more appropriate criterion.

Four PCMs were utilized in the phase transition temperature range of 15–23 °C to determine the appropriate temperature for the storage tank. Besides, a water tank with the same mass was used to show the justification of the PCM storage tank. The maximum absorbed cooling power of 49.9 W/m$^2$ and the highest temperature drop of 14.8 °C were measured for 23 °C and 15 °C PCM tanks, respectively.

The 18 °C PCM tank with the maximum exergy efficiency of 42.8% and average exergy efficiency of 33.7% had the greatest amount relative to the other tanks. Although 23 °C PCM had the highest average energy efficiency of 65.3%, its average exergy efficiency of 31.5% was lower than other PCMs but higher than the water tank with 28.6% efficiency.

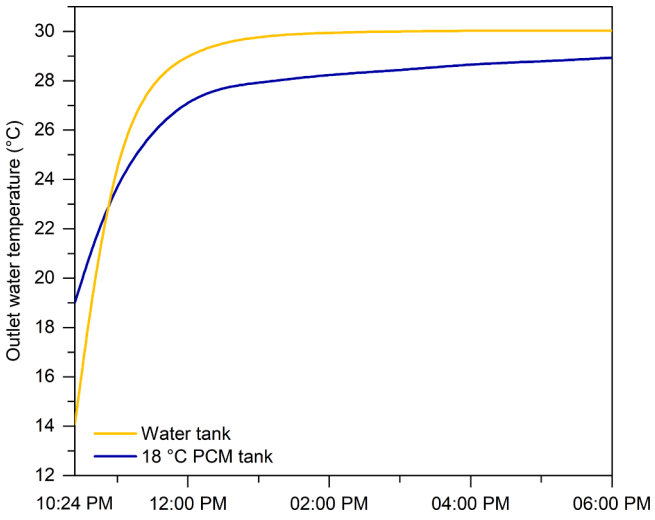


**Fig. 9.** Outlet water temperature of 18 °C PCM and water tanks during the discharge process.

The minimum and maximum ambient temperatures on the studied day were 27 °C and 39 °C, respectively. Obviously, water cooling at higher temperatures will result in better cooling power. However, since the minimum ambient or tap water temperatures are infinitely available at midnight, the critical point is that the cold tank must reach a lower temperature. This is when using RSC systems is justified. The final temperature of the 18 °C PCM tank was 18.14 °C, which was almost nine degrees below the minimum ambient temperature.

Although the use of PCM has increased the exergy efficiency of the system, more studies are required to make this comparison in other climatic conditions to prove its justifiability throughout the year. Future studies will compare the economic feasibility of PCM-based PVT-RSC systems in different locations. Using RSC as a supplement can further develop PVT systems and reduce their levelized cost of energy.

### *CRediT authorship contribution statement*

**Soroush Kiyaee:** Conceptualization, Methodology, Formal analysis, Software, Validation, Investigation, Writing – original draft, Writing – review & editing. **Pooria Khalilmoghadam:** Conceptualization, Investigation, Methodology, Software. **Mohammad Behshad Shafii:** Supervision, Methodology, Writing – review & editing. **Alireza Z. Moshfegh:** Supervision, Project administration, Writing – review & editing, Funding acquisition. **Mingke Hu:** Conceptualization, Validation, Supervision, Project administration, Writing – review & editing, Funding acquisition.

### Declaration of Competing Interest

The authors declare that they have no known competing financial interests or personal relationships that could have appeared to influence the work reported in this paper.

### Acknowledgments

This study was sponsored by the H2020 Marie Skłodowska-Curie Actions - Individual Fellowships (842096), National Natural Science Foundation of China (NSFC 51906241), and Anhui Provincial Natural Science Foundation (1908085ME138). Partial support of Sharif University of Technology and Iran National Science Foundation through the

Chair of Surface/Interface Project (940009) is acknowledged.

## References


[1] Xu Y, Ramanathan V, Victor DG. Global warming will happen faster than we think. Nature 2018;564(7734):30–2. https://doi.org/10.1038/d41586-018-07586-5.

[2] Kiyaee S, Saboohi Y, Moshfegh AZ. A new designed linear Fresnel lens solar concentrator based on spectral splitting for passive cooling of solar cells. Energy Convers Manage 2021;230:113782. https://doi.org/10.1016/j.enconman.2020.113782.

[3] Faraji M, Yousefi M, Yousefzadeh S, Zirak M, Naseri N, Jeon TH, et al. Two-dimensional materials in semiconductor photoelectrocatalytic systems for water splitting. Energy Environ Sci 2019;12(1):59–95.

[4] Goldstein EA, Raman AP, Fan S. Sub-ambient non-evaporative fluid cooling with the sky. Nat Energy 2017. https://doi.org/10.1038/nenergy.2017.143.

[5] Shi J, Han D, Li Z, Yang Lu, Lu S-G, Zhong Z, et al. Electrocaloric Cooling Materials and Devices for Zero-Global-Warming-Potential. High-Efficiency Refrig Joule 2019;3(5):1200–25. https://doi.org/10.1016/j.joule.2019.03.021.

[6] Fan S, Raman A. Metamaterials for radiative sky cooling. Natl Sci Rev 2018;5(2):132–3. https://doi.org/10.1093/nsr/nwy012.

[7] Zhao D, Martini CE, Jiang S, Ma Y, Zhai Y, Tan G, et al. Development of a single-phase thermosiphon for cold collection and storage of radiative cooling. Appl Energy 2017;205:1260–9. https://doi.org/10.1016/j.apenergy.2017.08.057.

[8] Zhao B, Pei G, Raman AP. Modeling and optimization of radiative cooling based thermoelectric generators. Appl Phys Lett 2020;117(16):163903. https://doi.org/10.1063/5.0022667.

[9] Liu J, Zhang Ji, Tang H, Zhou Z, Zhang D, Ye L, et al. Recent advances in the development of radiative sky cooling inspired from solar thermal harvesting. Nano Energy 2021;81:105611. https://doi.org/10.1016/j.nanoen.2020.105611.

[10] Zhao D, Aili A, Zhai Y, Xu S, Tan G, Yin X, et al. Radiative sky cooling: Fundamental principles, materials, and applications. Appl Phys Rev 2019;6(2):021306. https://doi.org/10.1063/1.5087281.

[11] Catalanotti S, Cuomo V, Piro G, Ruggi D, Silvestrini V, Troise G. The radiative cooling of selective surfaces. Sol Energy 1975;17(2):83–9. https://doi.org/10.1016/0038-092X(75)90062-6.

[12] Granqvist CG, Hjortsberg A. Radiative cooling to low temperatures: General considerations and application to selectively emitting SiO films. J Appl Phys 1981;52(6):4205–20. https://doi.org/10.1063/1.329270.

[13] Gentle AR, Smith GB. Radiative heat pumping from the Earth using surface phonon resonant nanoparticles. Nano Lett 2010;10(2):373–9. https://doi.org/10.1021/nl903271d.

[14] Hosseinzadeh E, Taherian H. An experimental and analytical study of a radiative cooling system with unglazed flat plate collectors. Int J Green Energy 2012;9(8):766–79. https://doi.org/10.1080/15435075.2011.641189.

[15] Wang T, Wu Yi, Shi L, Hu X, Chen M, Wu L. A structural polymer for highly efficient all-day passive radiative cooling. Nat Commun 2021;12(1). https://doi.org/10.1038/s41467-020-20646-7.

[16] Chen Z, Zhu L, Raman A, Fan S. Radiative cooling to deep sub-freezing temperatures through a 24-h day-night cycle. Nat Commun 2016;7(1). https://doi.org/10.1038/ncomms13729.

[17] Zhao D, Aili A, Zhai Y, Lu J, Kidd D, Tan G, et al. Subambient Cooling of Water: Toward Real-World Applications of Daytime Radiative Cooling. Joule 2019;3(1):111–23. https://doi.org/10.1016/j.joule.2018.10.006.

[18] Vall S, Medrano M, Solé C, Castell A. Combined Radiative Cooling and Solar Thermal Collection: Experimental Proof of Concept n.d. https://doi.org/10.3390/en13040893.

[19] Hu M, Zhao B, Ao X, Suhendri, Cao J, Wang Q, et al. An analytical study of the nocturnal radiative cooling potential of typical photovoltaic/thermal module. Appl Energy 2020;277:115625. https://doi.org/10.1016/j.apenergy.2020.115625.

[20] Bokor B, Akhan H, Eryener D, Horváth M. Nocturnal passive cooling by transpired solar collectors. Appl Therm Eng 2021;188:116650. https://doi.org/10.1016/j.applthermaleng.2021.116650.

[21] Kazemian A, Salari A, Hakkaki-Fard A, Ma T. Numerical investigation and parametric analysis of a photovoltaic thermal system integrated with phase change material. Appl Energy 2019;238:734–46. https://doi.org/10.1016/j.apenergy.2019.01.103.

[22] Eisapour M, Eisapour AH, Hosseini MJ, Talebizadehsardari P. Exergy and energy analysis of wavy tubes photovoltaic-thermal systems using microencapsulated PCM nano-slurry coolant fluid. Appl Energy 2020;266:114849. https://doi.org/10.1016/j.apenergy.2020.114849.

[23] Li X, Duan J, Simon T, Ma T, Cui T, Wang Q. Nonuniform metal foam design and pore-scale analysis of a tilted composite phase change material system for photovoltaics thermal management. Appl Energy 2021;298:117203. https://doi.org/10.1016/j.apenergy.2021.117203.

[24] Eicker U, Dalibard A. Photovoltaic–thermal collectors for night radiative cooling of buildings. Sol Energy 2011;85(7):1322–35.

[25] Zhang S, Niu J. Cooling performance of nocturnal radiative cooling combined with microencapsulated phase change material (MPCM) slurry storage. Energy Build 2012;54:122–30. https://doi.org/10.1016/J.ENBUILD.2012.07.041.

[26] Yu C, Shen D, He W, Hu Z, Zhang S, Chu W. Parametric analysis of the phase change material wall combining with micro-channel heat pipe and sky radiative cooling technology. Renew Energy 2021;178:1057–69. https://doi.org/10.1016/J.RENENE.2021.07.001.

[27] Kwan TH, Gao D, Zhao B, Ren X, Hu T, Dabwan YN, et al. Integration of radiative sky cooling to the photovoltaic and thermoelectric system for improved space cooling. Appl Therm Eng 2021;196:117230. https://doi.org/10.1016/j.applthermaleng.2021.117230.

[28] Liu J, Yuan J, Zhang Ji, Tang H, Huang Ke, Xing J, et al. Performance evaluation of various strategies to improve sub-ambient radiative sky cooling. Renew Energy 2021;169:1305–16. https://doi.org/10.1016/j.renene.2021.01.103.

[29] Zhang K, Zhao D, Yin X, Yang R, Tan G. Energy saving and economic analysis of a new hybrid radiative cooling system for single-family houses in the USA. Appl Energy 2018;224:371–81. https://doi.org/10.1016/j.apenergy.2018.04.115.

[30] Hu M, Zhao B, Ao X, Ren X, Cao J, Wang Q, et al. Performance assessment of a trifunctional system integrating solar PV, solar thermal, and radiative sky cooling. Appl Energy 2020;260:114167. https://doi.org/10.1016/j.apenergy.2019.114167.

[31] Gallardo A, Berardi U. Design and control of radiant ceiling panels incorporating phase change materials for cooling applications. Appl Energy 2021;304:117736.

[32] PureTemp LLC. PureTemp PCMs 2021. https://puretemp.com/?p=220 (accessed October 18, 2021).

[33] Ahmadkhani MB. Traditional Sustainable Solutions in Iranian Desert Architecture to Solve the Energy Problem. Int J "Tech Phys Probl Eng" (IJTPE) 2011.

[34] Iran Meteorological Organization. Yazd weather synoptic data 2020. https://data.irimo.ir/.

[35] Berk A, Conforti P, Kennett R, Perkins T, Hawes F, van den Bosch J. MODTRAN6: a major upgrade of the MODTRAN radiative transfer code. Algorithms and Technologies for Multispectral, Hyperspectral, and Ultraspectral Imagery XX, 2014. https://doi.org/10.1117/12.2050433.

[36] Huang Z, Ruan X. Nanoparticle embedded double-layer coating for daytime radiative cooling. Int J Heat Mass Transf 2017;104:890–6. https://doi.org/10.1016/j.ijheatmasstransfer.2016.08.009.

[37] Zhao B, Hu M, Ao X, Chen N, Xuan Q, Jiao D, et al. Performance analysis of a hybrid system combining photovoltaic and nighttime radiative cooling. Appl Energy 2019;252:113432. https://doi.org/10.1016/j.apenergy.2019.113432.

[38] Hu M, Pei G, Wang Q, Li J, Wang Y, Ji J. Field test and preliminary analysis of a combined diurnal solar heating and nocturnal radiative cooling system. Appl Energy 2016;179:899–908. https://doi.org/10.1016/j.apenergy.2016.07.066.

[39] COMSOL Multiphysics v. 5.5. Heat Transfer Module User's Guide. COMSOL AB, Stockholm, Sweden: 2019.

[40] Incropera FP, DeWitt DP, Bergman TL, Lavine AS. Fundamentals of Heat and Mass Transfer(6th edition). 2007. https://doi.org/10.1016/j.applthermaleng.2011.03.022.

[41] Dincer I, Zamfirescu C. Fundamental Aspects. Sustainable Hydrogen. Production 2016:1–63. https://doi.org/10.1016/B978-0-12-801563-6.00001-7.

[42] Tiwari A, Dubey S, Sandhu GS, Sodha MS, Anwar SI. Exergy analysis of integrated photovoltaic thermal solar water heater under constant flow rate and constant collection temperature modes. Appl Energy 2009;86(12):2592–7. https://doi.org/10.1016/j.apenergy.2009.04.004.

[43] Yumrutaş R, Kunduz M, Kanoğlu M. Exergy analysis of vapor compression refrigeration systems. Exergy, Int J 2002;2(4):266–72.

[44] Kambezidis HD. The Solar Resource. Comprehensive. Renew Energy 2012;3:27–84. https://doi.org/10.1016/B978-0-08-087872-0.00302-4.

[45] Croda International Plc. CrodaTherm™ 21 2022. https://www.crodaenergytechnologies.com/en-gb/product-finder/product/979-CrodaTherm_1_21 (accessed January 23, 2022).